IEEE Access
Multidisciplinary | Rapid Review | Open Access Journal

Received October 16, 2018, accepted October 31, 2018, date of publication November 12, 2018,
date of current version December 7, 2018.

Digital Object Identifier 10.1109/ACCESS.2018.2880845

Bionic Algorithm for Color Fusion of Infrared and Low Light Level Image Based on Rattlesnake Bimodal Cells

ZHEN ZHANG[1,2], HUIQI LI[1], AND GUORU ZHAO[1]
[1]CAS Key Laboratory of Health Informatics, Shenzhen Institutes of Advanced Technology, Chinese Academy of Sciences, Shenzhen 518055, China
[2]School of Information Engineering, Wuhan University of Technology, Wuhan 430070, China

Corresponding author: Guoru Zhao (gr.zhao@siat.ac.cn)

This work was supported in part by the National Natural Science Foundation of China under Grant 61761166007 and Grant 71532014, in part by the Key Program for the Guangdong Science and Technology Development Fund under Grant 2015B020233011, and in part by the Shenzhen Science and Technology Development Fund under Grant JCYJ20170818163505850.

ABSTRACT Night vision technology is becoming ever-more widely used in military and civil fields, and it will be more accurate for target detection and recognition through color fusion of infrared and low light level images. Since the classic Waxman fusion model-only simulates the rattlesnake's IR-depressed Visual Cell and the target in fusion image is not obvious, a novel fusion model is proposed in this paper. We enhance the edge information through the ON neural network for the infrared and low light-level images and then establish a mathematical model to process the rattlesnake's "enhanced cells" and "depressed cells". Next, we input the ON-central receptive field for fusion and RGB spatial mapping, which can fully realize the union function of the "enhanced cells" and "depressed cells". Finally, we conduct comparative experiments and image quality evaluation with the classical Waxman fusion model. The results show that image targets are more obvious obtained by our algorithm and increased by an average of 51.97%, 4.07%, and 7.62% than Waxman algorithm in terms of color, mutual information, and structural similarity, respectively. It turned out that our fusion images are richer in color than the Waxman fusion images, which contain more source image information, and more similar to the source image structure.

INDEX TERMS Infrared image, low light level image, color fusion, bionic, bimodal cell.

I. INTRODUCTION

Night vision technology was proposed by the US Department of Defense in the 1930s and is mainly used for military activities. However, it is gradually being applied more in the civilian field along with the continuous development and improvement of night vision technology. There are some of the most common applications, such as night driving or flying, night safety monitoring, wildlife observation, sleep laboratory monitoring and search and rescue, etc.

The color night vision technology, which can utilize a variety of sensor image information of multi-spectral night vision systems (infrared and low light level image) to form a unified color night vision image. In the color night vision technology, the target and the background can be recognized not only by the brightness but also by the chromatic aberration, which help to improve the image quality of the night vision system, the response speed of the observer and the ability of target recognition, and it also enhance the performance of the night vision system greatly. Therefore, it is of great practical significance to carry out a series of research on color fusion methods of infrared and LLL (low light level) images.

In 2000, Allen M. Waxman and David A. Fay of the MIT obtained natural color fusion images based on Opponent Receptive Field Theory by simulating the two-channel visual characteristics of the rattlesnake to fuse infrared and LLL images.

In 1996, Alexander Toet of the Netherlands Organization for Applied Scientific Research developed a TNO method [3] by using the unique and common features of infrared and LLL images for fusion. In 2003, Toet [4] used Reinhard color transfer algorithm to color remapping the image obtained by TNO method. In 2008, Toet and Hogervorst [5], [6] proposed to use the look-up table method to carry out the color fusion method of infrared and LLL images, whereas it needs much more prior information and limits its usage in night vision. In 2010, Li *et al.* [7] obtained a better fusion image by using color space YC_bC_r instead of color transfer $l\alpha\beta$ and greatly reduced the complexity of the Toet color transfer

fusion algorithm. In 2012, Qian *et al.* [8] proposed a fast color fusion method for local color transfer. In 2016, Qu *et al.* [9] used the GIST (Generalized Search Trees) feature of infrared and LLL images to classify the scenes, and then selected the appropriate color reference images from the image library for color transfer. In 2017, Lu *et al.* [10] proposed a method based on scene parsing to select the appropriate color reference image for color transfer.

It can be seen that the current infrared and LLL color fusion algorithm mainly focus on the Waxman fusion method and the color transfer method. However, the color transfer algorithm relies too much on the reference image, and the algorithm is complicated and difficult to implement. Although the Waxman fusion method can obtain a more natural color image, the target is difficult to recognize. In this paper, we propose a new bionic algorithm for color fusion based on rattlesnake bimodal cells.

The main structure of the article is as follows: In section 2, we first introduce the concentric circle opponent receptive field and the rattlesnake bimodal cells, Secondly, we analyze the process of Waxman fusion method in detail and point out the defects of Waxman method. In section 3, we first conduct the mathematical modeling and simulation of the rattlesnake bimodal cells, and then propose a new bionic algorithm for color fusion. In section 4, we evaluate the fusion results obtained by our method and Waxman method.

II. WAXMAN COLOR FUSION ALGORITHM

Waxman *et al.* were inspired by the rattlesnake. They used the concentric circle opponent receptive field to fuse infrared and LLL images. Although the natural color image could be obtained, the target was not prominent.

A. RECEPTIVE FIELD MATHEMATICAL MODEL

Physiological vision studies show that the spatial distribution of the retinal receptive field is a concentric circular opponent receptive field model, which can be divided into two systems: ON-center/OFF-surround system and OFF-center/ON-surround system. The two receptive field models are shown in Fig. 1, where the "+" represents the excitatory receptive field and the "−" represents the inhibitory receptive field.

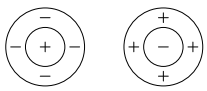

FIGURE 1. ON-Center Receptive Field (left) and OFF-Center Receptive Field (right).

The passive membrane equation is a kinetic description of the center-surround antagonistic domain and is primarily used to simulate electrophysiological cell membrane ion exchange, originally proposed by A.L. Hodgkin and A.F. Huxley. The most widely used method is the passive membrane dynamics equation established by Grossberg for concentric circles to antagonize structural receptive fields. The derivation process of the ON-center type receptive field passive membrane dynamic equation is as follows.

In general, each population contains both excitatory and sleeping subpopulations of cells, and the two kind of cells are convertible at any time. The excitable sites cells generate a pulse frequency, and the sleeping state cells do not generate a pulse frequency. Let $x(t)$ be the number of pulse frequency generated by all cells at time t. Three effects determine the passive membrane dynamics equation:

1) Spontaneous Decay Activity of Cells

Active sites become inactive at a fixed rate. Assuming that the rate is A, then the spontaneous decay pulse of the cell at time t is $A[x(t)-D]$. Where A is a constant and D is the basal cell activity.

2) Inhibition Activity of Excitatory Cells

The frequency at which excitatory cells release pulse is depressed by a randomly distributed inhibition signal $S(t)$, and the intensity is proportional to $[F + x(t)]S(t)$. Where $S(t)$ is an externally inhibition signal, and F is a polarization constant.

3) Triggered Activity of Sleeping Cells

The sleeping cells are activated by a randomly distributed excitation signal $C(t)$, which becomes an excited state and begins to release pulse, and the intensity is proportional to $[E - x(t)]C(t)$. Where $C(t)$ is the external excitation signal, and E is a polarization constant.

The passive membrane dynamics equation is obtained from the above three factors:

$$\frac{d}{dt}x = -A[x(t)-D]+[E-x(t)]C(t)-[F+x(t)]S(t) \quad (1)$$

When the equation is balanced, there are:

$$x = \frac{AD + EC(t) - FS(t)}{A + C(t) + S(t)} \quad (2)$$

Therefore, the ON-center receptive field equation [11] is:

$$x_{i,j} = \left[\frac{AD + EC_{i,j} - FS_{i,j}}{A + C_{i,j} + S_{i,j}}\right]^+ \quad (3)$$

The OFF-center receptive field equation [11] is:

$$\tilde{x}_{i,j} = \left[\frac{A\tilde{D} + ES_{i,j} - FC_{i,j}}{A + C_{i,j} + S_{i,j}}\right]^+ \quad (4)$$

Where i, j is the pixel coordinate and A is the attenuation constant and $D, \tilde{D}$ are the basal activity of cells, E and F are polarization constants. $[]^+$ represents the rectifier, that is $[x]^+ = \max(x, 0)$. Center area of receptive field $C_{i,j}$ and surrounding area of receptive field $S_{i,j}$ are:

$$C_{i,j} = I^c_{i,j} * G_c(m,n) = \frac{1}{\sqrt{2\pi\sigma_c^2}} \sum_{m,n} I^c_{i-m,j-n} \exp\left(-\frac{m^2+n^2}{2\sigma_c^2}\right) \quad (5)$$

$$S_{i,j} = I^s_{i,j} * G_s(p,q) = \frac{1}{\sqrt{2\pi\sigma_s^2}} \sum_{p,q} I^s_{i-p,j-q} \exp\left(-\frac{p^2+q^2}{2\sigma_s^2}\right) \quad (6)$$

Among them, $I^c_{i,j}$ and $I^s_{i,j}$ are the input images of the central area $C_{i,j}$ and the surrounding area $S_{i,j}$ respectively. $G_c(m, n)$ and $G_s(p, q)$ are the Gaussian distribution functions of the central area and the surrounding area respectively. The Gaussian function widths are σ_c, σ_s respectively, and the Gaussian template sizes are $m \times n$ and $p \times q$ respectively.

B. RATTLESNAKE BIMODAL CELL

The IR-depressed Visual Cell, Visual-depressed IR Cell, IR-enhanced Visual Cell and Visual-enhanced IR Cell of the bimodal cells in the rattlesnake optic tectum can fuse the infrared stimulation signal and the visible light stimulation signal to form the dual vision perceptual system of the rattlesnake [12].

1) "Depressed cells": responds only to one modal signal and does not respond when stimulated only by another model signal. However, the neuronal cell response will be inhibited and significantly weakened when neuronal cells are co-stimulated by two kinds of modal signals. "Depressed cells" are composed of two kinds of cells, namely "Visual-depressed IR Cell" and "IR-depressed Visual Cell".
2) "Enhanced cells": respond only to one modal signal and does not respond when stimulated only by another modal signal. However, the neuronal cell response will be enhanced and become significantly stronger when neuronal cells are co-stimulated by two modal signals. "Enhanced cells" are also composed of two types of cells, namely "Visual-enhanced IR Cell" and "IR-enhanced Visual Cell".

C. WAXMAN FUSION STRUCTURE

The Waxman fusion structure is shown in Fig. 2. In the first stage of the algorithm, they use the ON system to enhance the edge information of the infrared and LLL image and then obtain the *ON_IR* and *ON_LLL* image. And then use the OFF system to enhance the edge information of the infrared image, darken the bright area and brighten the dark area to get the *OFF_IR* image. In the second stage, *ON_LLL* and *ON_IR* are fed into the excitatory and inhibitory center of the ON-center receptive field respectively, and then the fusion signal $+LLL - IR$ is obtained to simulate the IR-depressed Visual Cell. Then *ON_LLL* and *OFF_IR* are fed into the excitatory and inhibitory center of the ON-center receptive field respectively, and then the fusion signal $+LLL + IR$ is obtained to simulate the IR-enhanced Visual Cell. In the third stage, the three signals $+LLL + IR$, *ON_LLL*, and $+LLL - IR$ are mapped to the *R*, *G*, and *B* three color channels respectively to generate a color fusion image.

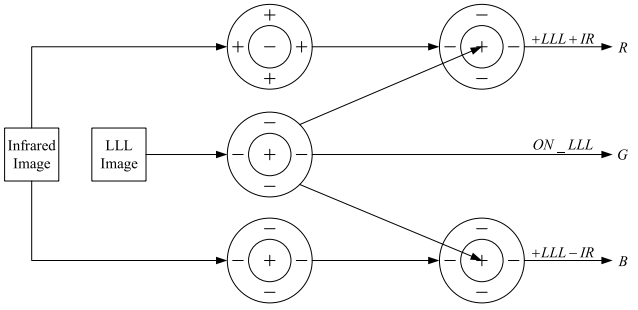

FIGURE 2. Waxman fusion structure.

Since the *OFF_IR* only darkens the original infrared signal at the bright place and brightens the dark place, it is still a signal that is always greater than or equal to zero, so the enhanced signal $+LLL + IR$ which obtained by feeding *ON_LLL* into the excitatory center and *OFF_IR* into the inhibitory center is still the depressed signal. Therefore, the Waxman fusion method only simulated the IR-depressed Visual Cell of the rattlesnake, and the rest of them are not simulated, so the "integrity" of the rattlesnake bimodal cells cannot be reflected. And also the fusion image obtained by Waxman method is not obvious.

III. PROPOSED COLOR FUSION ALGORITHM

In view of the defects of the Waxman method, this section builds a model based on the "depressed cells" and "enhanced cells" of the rattlesnake and proposes a new color fusion method.

A. MATHEMATICAL MODEL OF RATTLESNAKE BIMODAL CELL

There are two kinds of rattlesnake bimodal cell: depressed and enhanced cell. In this paper, mathematical modeling is carried out respectively.

1) DEPRESSED CELLS

The Waxman fusion method shows that the passive membrane equation of the ON-central receptive field can be used to simulate "depressed cells."

$$f_{A\to B^-}(i,j) = \left[\frac{AD + EC_{i,j} - FS_{i,j}}{A + C_{i,j} + S_{i,j}}\right]^+ \tag{7}$$

Where $f_{A\to B^-}$ means that the signal A depressed the signal B. The $C_{i,j}$ and $S_{i,j}$ are:

$$C_{i,j} = f_B{}^* G_c(m,n) = \frac{1}{\sqrt{2\pi\sigma_c^2}} \sum_{m,n} f_B \exp(-\frac{m^2+n^2}{2\sigma_c^2}) \tag{8}$$

$$S_{i,j} = f_A{}^* G_s(p,q) = \frac{1}{\sqrt{2\pi\sigma_s^2}} \sum_{p,q} f_A \exp(-\frac{p^2+q^2}{2\sigma_s^2}) \tag{9}$$

Where the f_A and f_B represent the signal A and B respectively.

Fig. 3 is a waveform diagram of input signal 1 and 2, the waveforms of "Depressed cells" are only stimulated by signal 1, "Depressed cells" are only stimulated by signal 2, and "Depressed cells" are co-stimulated by signal 1 and 2 are shown in Fig. 4.

As can be seen from Fig. 4, when "Depressed cells" are only stimulated by signal 1, the mathematical model of "Depressed cells" has corresponding output signal; when "Depressed cells" are only stimulated by signal 2,

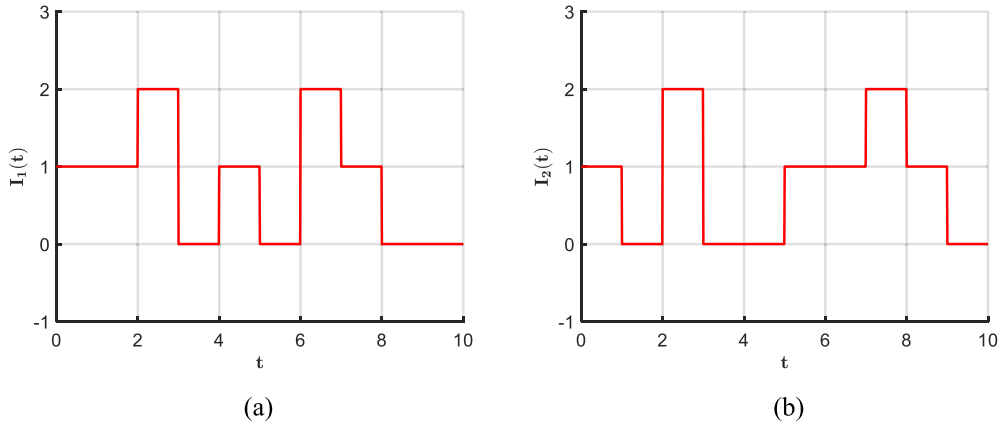

FIGURE 3. Input signal waveform. (a) Input signal 1, (b) Input signal 2.

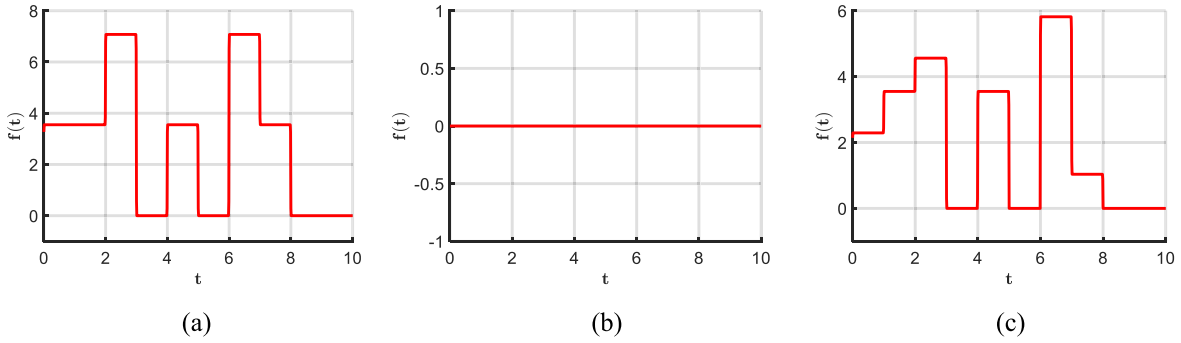

FIGURE 4. Response waveform of Depressed cells. (a) Stimulated by signal 1 only, (b) Stimulated by signal 2 only, (c) Co-stimulated by signal 1 and 2.

the output signal of "Depressed cells" mathematical model is 0; when "Depressed cells" are co-stimulated by signal 1 and 2, the mathematical model of "Depressed cells" has corresponding output signal, and the larger input signal 2 is, the smaller output signal is, which means that the signal 2 has a restraining effect on the signal 1. This characteristic accords with the rattlesnake's "Depressed cells" biological model.

2) ENHANCED CELLS

Similarly, assuming that $x(t)$ is the number of active sites at time t, the mathematical model of "enhanced cells" is determined by three factors:

1) Spontaneous Decay Activity of Cells

Active sites become inactive at a fixed rate. Assuming that the rate is A, then the spontaneous decay pulse of the cell at time t is $A[x(t) - D]$. Where A is a constant and D is the basal cell activity.

2) Enhancement Activity of Excitatory Cells

The frequency at which excitatory cells release pulse is enhanced by a randomly distributed enhancement signal $S(t)$, and the intensity is proportional to $[F + x(t)]S(t)$. Where $S(t)$ is an externally enhanced signal, and F is a polarization constant.

3) Triggered Activity of Sleeping Cells

The sleeping cells are activated by a randomly distributed excitation signal $C(t)$, which becomes an excited state and begins to release pulse, and the intensity is proportional to $[E - x(t)]C(t)$. Where $C(t)$ is the external excitation signal, and E is a polarization constant.

The mathematical model of "enhanced cells" is obtained from the above three factors:

$$\frac{d}{dt}x = -A[x(t) - D] + [E - x(t)]C(t) + [F + x(t)]S(t) \tag{10}$$

When the system is balanced, the equation is:

$$x = \frac{AD + EC(t) + FS(t)}{A + C(t) - S(t)} \tag{11}$$

Therefore, the mathematical model of "enhanced cells" is shown in (12).

$$f_{A\to B^+}(i,j) = \begin{cases} \left[\dfrac{AD + EC_{i,j} + FS_{i,j}}{A + C_{i,j} - S_{i,j}}\right]^+, & \textit{signal A exists} \\ 0, & \textit{signal A does not exist} \end{cases} \tag{12}$$

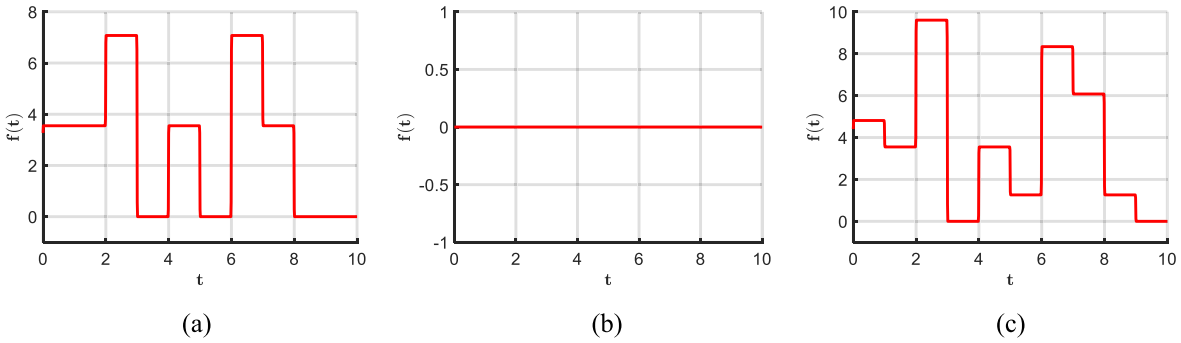

FIGURE 5. Response waveform of Enhanced cells. (a) Stimulated by signal 1 only, (b) Stimulated by signal 2 only, (c) Co-stimulated by signal 1 and 2.

Where $f_{A\to B^+}$ means that the signal A enhanced the signal B. The $C_{i,j}$ and $S_{i,j}$ are:

$$C_{i,j} = f_B{}^* G_c(m,n) = \frac{1}{\sqrt{2\pi\sigma_c^2}} \sum_{m,n} f_B \exp(-\frac{m^2+n^2}{2\sigma_c^2}) \quad (13)$$

$$S_{i,j} = f_A{}^* G_s(p,q) = \frac{1}{\sqrt{2\pi\sigma_s^2}} \sum_{p,q} f_A \exp(-\frac{p^2+q^2}{2\sigma_s^2}) \quad (14)$$

Where the f_A and f_B represent the signal A and B respectively.

Fig. 3 is a waveform diagram of input signal 1 and 2, the waveforms of ''Enhanced cells'' are only stimulated by signal 1, ''Enhanced cells'' are only stimulated by signal 2, and ''Enhanced cells'' are co-stimulated by signal 1 and 2 are shown in Fig. 5.

As can be seen from Fig. 5, when ''Enhanced cells'' are only stimulated by signal 1, the mathematical model of ''Enhanced cells'' has corresponding output signal; when ''Enhanced cells'' are only stimulated by signal 2, the output signal of ''Enhanced cells'' mathematical model is 0; when ''Enhanced cells'' are co-stimulated by signal 1 and 2, the mathematical model of ''Enhanced cells'' has corresponding output signal, and the larger input signal 2 is, the larger output signal is, which means that the signal 2 has an enhancement effect on the signal 1. This characteristic accords with the rattlesnake's ''Enhanced cells'' biological model.

B. THE FUSION STRUCTURE OF PROPOSED ALGORITHM

The ''Enhanced cells'' model and the ''Depressed cells'' model (ON-central receptive field) are shown in Fig. 6.

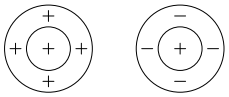

FIGURE 6. ''Enhanced cells'' model (left) and ''Depressed cells'' model (right).

The color fusion algorithm proposed in this paper has the following four stages: enhancement stage of edge information of the ON neural network, processing stage of the rattlesnake's ''enhanced cells'' and ''depressed cells'', fusion stage of the ON neural network, and the *RGB* spatial mapping stage. The color fusion structure proposed in this paper is shown in Fig. 7.

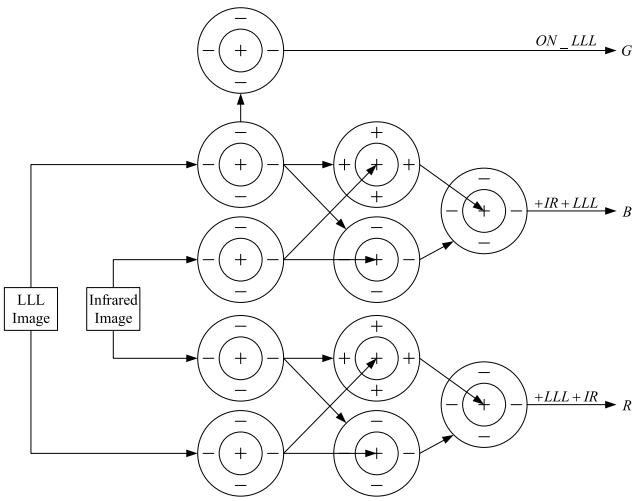

FIGURE 7. Color fusion structure.

The first stage of the algorithm—enhancement stage of edge information of the ON neural network—is the same as the Waxman fusion method. Both of them use the ON neural network to enhance the edge information of infrared and LLL images and obtain the *ON_IR* and *ON_LLL* image.

The second stage is the processing stage of the rattlesnake's ''enhanced cells'' and ''depressed cells''. At this stage, we feed *ON_IR* and *ON_LLL* into the central excitatory and surrounding enhanced region of the ''enhanced cells'' respectively to imitate the response of Visual-enhanced IR Cell and obtain the LLL enhanced infrared image $LLL \rightarrow IR^+$. We feed *ON_IR* and *ON_LLL* into the central excitatory and surrounding inhibitory region of the ''depressed cells'' respectively to imitate the response of Visual-depressed IR Cell and obtain the LLL depressed infrared image $LLL \rightarrow IR^-$. We feed *ON_LLL* and *ON_IR* into the central excitatory and surrounding enhanced region of the ''enhanced cell'' respectively to imitate the response

of IR-enhanced Visual Cell and obtain the infrared enhanced LLL image $IR \rightarrow LLL^{+}$. Finally, we feed ON_LLL and ON_IR into the central excitatory and surrounding depressed region of the ''depressed cell'' respectively to imitate the response of IR-depressed Visual Cell and obtain the infrared depressed LLL image $IR \rightarrow LLL^{-}$.

The third stage is the Fusion stage. We feed the LLL enhanced infrared image $LLL \rightarrow IR^{+}$ and the LLL depressed infrared image $LLL \rightarrow IR^{-}$ into the excitatory and inhibitory area of the ON neural network respectively to obtain the fusion image $(IR \uparrow +LLL) - (IR \downarrow -LLL) = +IR + LLL$. In the same way, we feed the infrared enhanced LLL image $IR \rightarrow LLL^{+}$ and the infrared depressed LLL image $IR \rightarrow LLL^{-}$ into the excitatory and inhibitory area of the ON neural network respectively and get the fusion image $(LLL \uparrow +IR) - (LLL \downarrow -IR) = +LLL + IR$.

The fourth stage is the *RGB* spatial mapping stage, which maps the signals $+LLL + IR$, ON_LLL, and $+IR + LLL$ to the *R*, *G*, and *B* color channels respectively and then generate a color fusion image.

IV. EXPERIMENT AND ANALYSIS

In this section, five groups of infrared and LLL images are used for simulation experiments. The following figures show original images and fusion images using the Waxman method and our algorithm respectively. We choose five images of the TNO Multiband Image Collection [13], including Sandpath, Nato camp, House, Soldier behind smoke, and Kaptein 1123.

It can be seen from Fig. 8 to Fig. 12 that fusion images obtained by our algorithm have more highlighted targets and richer color, whereas the target in the fusion images obtained by the Waxman method is difficult to identify under a com-

(a) (b) (c) (d)

FIGURE 8. Sandpath. (a) Original IR image, (b) Original LLL image, (c) Fusion image of Waxman method, (d) Fusion image of our method.

(a) (b) (c) (d)

FIGURE 9. Nato camp. (a) Original IR image, (b) Original LLL image, (c) Fusion image of Waxman method, (d) Fusion image of our method.

(a) (b) (c) (d)

FIGURE 10. House. (a) Original IR image, (b) Original LLL image, (c) Fusion image of Waxman method, (d) Fusion image of our method.

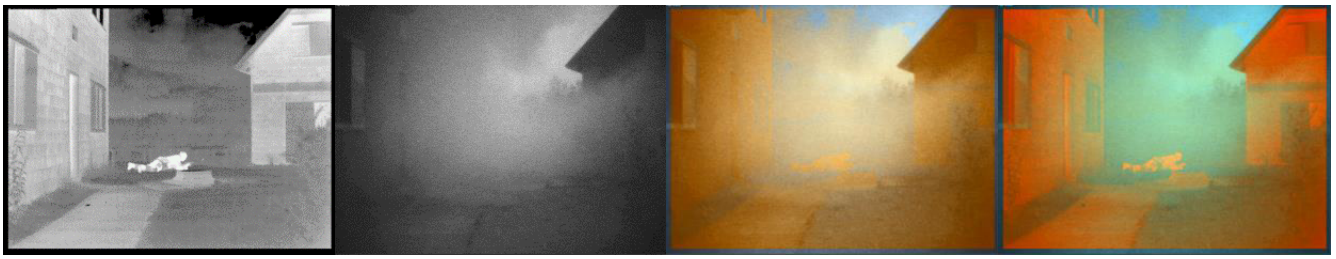

(a) (b) (c) (d)

FIGURE 11. Soldier behind smoke. (a) Original IR image, (b) Original LLL image, (c) Fusion image of Waxman method, (d) Fusion image of our method.

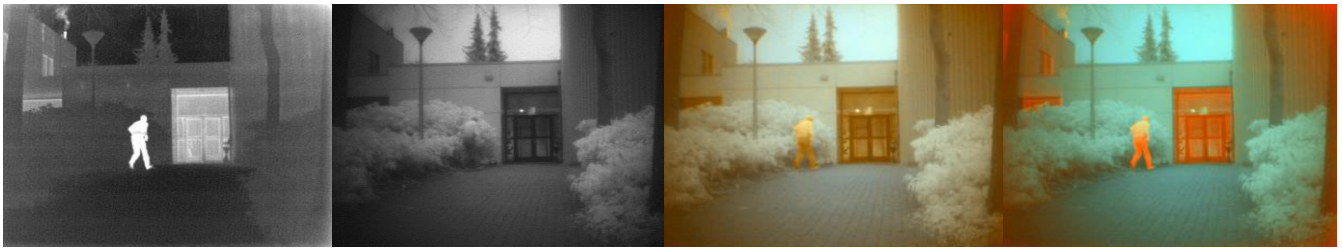

(a) (b) (c) (d)

FIGURE 12. Kaptein 1123. (a) Original IR image, (b) Original LLL image, (c) Fusion image of Waxman method, (d) Fusion image of our method.

TABLE 1. The evaluation results of two color fusion images.

Evaluation methods / Images	Gray Standard Deviation		Information Entropy		Average Gradient		Colorfulness	
	Waxman method	Our method	Waxman method	Our method	Waxman method	Our method	Waxman method	Our method
Sandpath	0.149	0.132	0.029	0.030	0.024	0.027	0.387	0.537
Nato camp	0.159	0.149	0.049	0.050	0.018	0.017	0.398	0.629
House	0.211	0.204	0.245	0.243	0.016	0.017	0.384	0.582
Soldier behind smoke	0.201	0.199	0.112	0.113	0.015	0.016	0.641	0.957
Kaptein 1123	0.197	0.187	0.078	0.079	0.011	0.012	0.459	0.735

plicated environmental condition. For instance, the target is disappeared in the jungle or smoke.

We evaluate the experimental results objectively in two aspects. One is the contrast between two color fusion images; the other is the contrast between the color fusion images and the original grayscale images.

A. COMPARISON AND EVALUATION AMONG COLOR FUSION IMAGES

The fusion image of Waxman method and our method both are three-channel images, which can be directly compared. Therefore, this paper evaluates the gray standard deviation, information entropy, average gradient, and colorfulness [14] of two color fused images. The results are shown in Table 1.

It can be seen from the table that the two algorithms in terms of gray standard deviation, information entropy and average gradient are almost the same. As for the colorfulness, however, the fusion image of our algorithm is higher than the Waxman algorithm by 41.10%, 57.91%, 51.52%, 49.24% and 60.07% respectively in five different scenes. These results indicating that the fusion image of our algorithm has better color performance, which can display more kinds of colors and more information.

B. COMPARISON AND EVALUATION BETWEEN COLOR FUSION IMAGES AND ORIGINAL GRAYSCALE IMAGES

Since the color image is a three-channel image and the original grayscale image is a single-channel image, it cannot be evaluated directly. Therefore, we convert the color of *RGB* space into color of *YIQ* space, which is similar to human perception, and compare the luminance channel Y of the fusion images with the original gray images by using the evaluation methods of mutual information [15] and SSIM (structural similarity index) [16]. The results are shown in Table 2.

It can be seen from the table that the mutual information between the fusion images obtained by our algorithm and the original images is 3.29%, 5.28%, 3.28%, 4.30% and 4.17% higher than that obtained by the Waxman algorithm. The SSIM between the fusion images obtained by our algorithm and the original images is 9.44%,7.93%,7.39%,6.65% and 6.71% higher than that obtained by the Waxman algorithm.

TABLE 2. The evaluations between color fusion images and original grayscale images.

Evaluation methods / Images	Mutual Information		SSIM	
	Waxman method	Our method	Waxman method	Our method
Sandpath	0.8289	0.8562	0.5741	0.6283
Nato camp	0.8087	0.8514	0.6242	0.6737
House	0.8220	0.8490	0.6276	0.6740
Soldier behind smoke	0.8402	0.8763	0.6282	0.6700
Kaptein 1123	0.8152	0.8492	0.6547	0.6986

The fusion image obtained by our algorithm, whether in the value of mutual information or SSIM, always performs better than the fusion image obtained by Waxman method. It is shown that the fusion images obtained by our algorithm contain more information about original infrared and LLL images and their structures are more similar.

V. CONCLUSION

Based on the classical Waxman fusion model, we researched on the visual mechanism of rattlesnake and propose a new bionic algorithm for color fusion of Infrared and LLL image. In this paper, we compare our algorithm with the classical Waxman algorithm, and evaluated the image quality of fusion images. Evaluation results show that the fusion images obtained by our algorithm have more outstanding advantages. They have a richer color, more obvious targets and better comprehensive fusion effect.

ACKNOWLEDGMENT

(Zhen Zhang and Huiqi Li contributed equally to this paper.) The authors would like to thank all reviewers for their valuable comments.

REFERENCES

[1] D. A. Fay *et al.*, "Fusion of multi-sensor imagery for night vision: Color visualization, target learning and search," in *Proc. 3rd Int. Conf. Inf. Fusion*, Paris, France, vol. 1, Jul. 2000, p. TUD3/3-TUD310, doi: 10.1109/IFIC.2000.862702.

[2] W. D. Ross *et al.*, "Multi-sensor 3D image fusion and interactive search," in *Proc. 3rd Int. Conf. Inf. Fusion*, Paris, France, vol. 1, Jul. 2000, pp. TUC3-10–TUC3-17, doi: 10.1109/IFIC.2000.862685.

[3] A. Toet and J. Walraven, "New false color mapping for image fusion," *Opt. Eng.*, vol. 35, no. 3, pp. 650–658, 1996, doi: 10.1117/1.600657.

[4] A. Toet, "Natural colour mapping for multiband nightvision imagery," *Inf. Fusion*, vol. 4, no. 3, pp. 155–166, 2003, doi: 10.1016/S1566-2535(03)00038-1.

[5] A. Toet and M. A. Hogervorst, "Portable real-time color night vision," *Proc. SPIE*, vol. 6974, pp. 697402-1–697402-12, Mar. 2008, doi: 10.1117/12.775405.

[6] A. Toet and M. A. Hogervorst, "Progress in color night vision," *Opt. Eng.*, vol. 51, no. 1, p. 010901, 2012, doi: 10.1117/1.OE.51.1.010901.

[7] G.-X. Li, S.-Y. Xu, Y.-L. Zhao, and T.-Y. Sun, "Fast color image fusion based on color transfer technique," *Opt. Precis. Eng.*, vol. 18, pp. 1637–1647, Jul. 2010, doi: 10.3788/OPE.20101807.1637.

[8] X. Qian *et al.*, "Color night vision algorithm based on local color mapping," *J. Image Graph.*, vol. 17, pp. 90–94, May 2012.

[9] Z. Qu, G. Xiao, N. Xu, Z. Diao, and H. Jia-Zhou, "A novel night vision image color fusion method based on scene recognition," in *Proc. 19th Int. Conf. Inf. Fusion (FUSION)*, Heidelberg, Germany, Jul. 2016, pp. 1236–1243.

[10] J. Lu *et al.*, "Scene parsing method toward LLL-level/infrared color night vision," *Infr. Laser Eng.*, vol. 2, pp. 29–34, Aug. 2017, doi: 10.3788/IRLA201746.0804002.

[11] S. Grossberg, E. Mingolla, and J. Williamson, "Synthetic aperture radar processing by a multiple scale neural system for boundary and surface representation," *Neural Netw.*, vol. 8, nos. 7–8, pp. 1005–1028, 1995, doi: 10.1016/0893-6080(95)00079-8.

[12] E. A. Newman and P. H. Hartline, "Integration of visual and infrared information in bimodal neurons in the rattlesnake optic tectum," *Science*, vol. 213, pp. 789–791, Aug. 1981, doi: 10.1126/science.7256281.

[13] T. Alexander. (Aug. 23, 2017). The TNO multiband image collection. Figshare. Collection. [Online]. Available: https://figshare.com/collections/The_TNO_Multiband_Image_Collection/3860689

[14] D. Hasler and S. E. Suesstrunk, "Measuring colorfulness in natural images," *Proc. SPIE*, vol. 5007, pp. 87–95, Jun. 2003, doi: 10.1117/12.477378.

[15] H. Dong and L. Liu, "No-reference image quality assessment in mutual information domain," *J. Image Graph.*, vol. 19, pp. 484–492, Mar. 2014.

[16] Z. Wang, A. C. Bovik, H. R. Sheikh, and E. P. Simoncelli, "Image quality assessment: From error visibility to structural similarity," *IEEE Trans. Image Process.*, vol. 13, no. 4, pp. 600–612, Apr. 2004, doi: 10.1109/TIP.2003.819861.

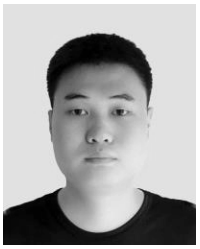

ZHEN ZHANG received the M.S. degree from the School of Information Engineering, Wuhan University of Technology, Wuhan, Hubei, China, in 2018. He was with the Shenzhen Institutes of Advanced Technology, Chinese Academy of Sciences, as a Research Assistant, from 2017 to 2018. He is currently at China Unicom, Shenzhen, Guangdong, China. His research interests include image processing and artificial intelligence.

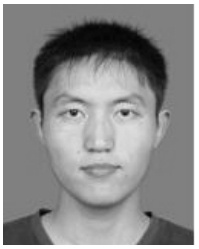

HUIQI LI received the M.Sc. degree from Shenzhen University, China, in 2012. He is currently an Engineer with the Shenzhen Institutes of Advanced Technology, Chinese Academy of Sciences. His current research interests mainly focus on night vision technology, body sensor networks, and wearable pre-impact fall systems.

GUORU ZHAO received the B.Sc., M.Sc., and Ph.D. degrees from Jilin University, China, in 2003, 2006, and 2009, respectively. He had studied in the Royal Veterinary College, University of London, U.K., as a Chinese Government Sponsored Scholar from 2007 to 2008. He is currently an Associate Professor with the Shenzhen Institutes of Advanced Technology, Chinese Academy of Sciences. His current research interests mainly focus on rehabilitation biomechanics and robotic systems, artificial intelligence algorithm, health care and safety monitoring for the elderly, and so on.